Plasmonics (2020) 15:1221–1229
https://doi.org/10.1007/s11468-020-01146-2

$BaTiO_3$-Graphene-Affinity Layer–Based Surface Plasmon Resonance (SPR) Biosensor for *Pseudomonas* Bacterial Detection

N. Mudgal[1] · Preecha Yupapin[2,3] · Jalil Ali[4] · G. Singh[1]

Received: 18 January 2020 / Accepted: 17 February 2020 / Published online: 2 March 2020

Abstract
In the present work, a highly sensitive SPR biosensor based on silver (Ag), barium titanate ($BaTiO_3$), graphene, and affinity layer is proposed for the detection of *Pseudomonas* bacteria. The performance of this proposed sensor has been numerically studied and analyzed for sensitivity, quality parameter, and detection accuracy. The proposed structure used attenuated total reflection (ATR) approach based on the Kretschmann configuration for the investigation of performance parameters. The inclusion of the $BaTiO_3$ layer along with the affinity layer shows the enhancement in the performance of the proposed structure for the detection of *Pseudomonas* bacteria. A comparison of the proposed structure is drawn with contemporary surface plasmon resonance (SPR) biosensors for the detection of *Pseudomonas* bacteria, and better performance was shown. This work reports that the maximum sensitivity, quality parameter, and detection accuracy for the proposed sensor are 220 degree/RIU, 101.38 RIU^{-1}, and 7.09 respectively. Therefore, the proposed design finds its application in *Pseudomonas* bacterial detection as well as opens a new window in the biosensing area.

Keywords Sensitivity · Biosensor · Barium titanate · Affinity layer · Surface plasmon resonance

Introduction

The genus *Pseudomonas* is a pervasive opportunistic pathogen widely found in soil, water, and nature. Most of the *Pseudomonas* species are saprophytic but some are linked with humans. These *Pseudomonas* species are the major cause of opportunistic infections in humans. The high fatality associated with such infections is due to the weakened antibiotic resistance, immune responses, and production of bacterial exoenzymes. Contaminated water and food are the possible ways of transmission of such bacteria [1–3]. A lot of research has been done already for the detection of this opportunistic bacteria. The surface plasmon resonance (SPR)-based sensors are increasing in demand in biosensing due to label-free sensing. Some of the biosensors based on SPR are already available for the detection of *Pseudomonas* bacteria but the advancement is still a prerequisite for the researchers [4–6]. In SPR-based biosensor, charge density oscillations of free electrons are generated at the interface of metal-dielectric surface, which are known as surface plasmons (SPs) and these can be excited by an incident light beam. This gives the formation of the evanescent wave that exponential decays along with the interface of the metal-dielectric surface. This collective event is known as surface plasmon resonance [7]. In recent years, SPR-based biosensors have received global attention from the wider scientific community due to their wide range of applications in the fields of biochemistry, environmental monitoring, and medicine, etc. [8–10]. In conventional prism-based SPR biosensor with a single metal, the sensitivity is low for the angular interrogation method but higher sensitivity is the ultimate goal of all researchers. Lately, SPR biosensors with a hybrid configuration of materials have been seen in research to improve the performance of SPR biosensors. These configurations of materials are the various combinations of metals and dielectrics depending upon the applications of SPR biosensors. In recent years, transition metal dichalcogenides (TMDCs) 2D nanomaterials, such as molybdenum disulfide

✉ N. Mudgal
mudgalnitesh@gmail.com

[1] Department of ECE, Malaviya National Institute of Technology Jaipur (MNIT), Jaipur, India

[2] Computational Optics Research Group, Advanced Institute of Materials Science, Ton Duc Thang University, District 7, Ho Chi Minh City, Vietnam

[3] Faculty of Applied Sciences, Ton Duc Thang University, District 7, Ho Chi Minh City, Vietnam

[4] Laser Centre, IBNU SINA ISIR, Universiti Teknologi Malaysia, 81310 Johor Bahru, Malaysia

(MoS_2), tungsten diselenide (WSe_2), and tungsten disulfide (WS_2), have been seen in SPR biosensing due to their remarkable optical properties [11–13]. The bonding of *Pseudomonas* with an affinity layer is an essential phenomenon for sensing. A large number of *Pseudomonas* bacterial attachment over the affinity layer was found for carbon sources toluene, nicotine, etc., as well as hydrophobic plastic especially polyethylene, Teflon, polystyrene, poly (ethylene terephthalate), etc., with no or little surface charge, while a moderate amount of *Pseudomonas* bacterial attachment to hydrophilic metals was found with a positive surface charge for platinum or neutral surface charge for germanium. Along with this, very little bacterial attachment was found for hydrophilic, negatively charged substrate (mica, glass, oxidized plastics) [14]. Lately, nanomaterials have been seen in emerging trends for biosensing due to a large surface area to volume ratio. Graphene is a nanomaterial of a single atomic layer, in which sp^2-hybridized carbon atoms are tightly packed in a 2D honeycomb lattice structure. The physical and structural characteristics of this material make graphene a promising nanomaterial in the biosensing field. The large surface area and strong interaction of π stacking with hexagonal cells show a very high absorption capability of the graphene layer. This makes graphene a suitable material for biomolecule adsorption [15–17]. The shifting of the resonance angle is a crucial phenomenon in the SPR sensor for enhancing the sensor performance. However, zinc oxide (ZnO) was utilized for improving the sensor performance but the large full width half maxima (FWHM) and the lower sensitivity are still major concerns in these structures [18, 19]. Recently, $BaTiO_3$ with remarkable properties, like low dielectric losses, high refractive index, and high dielectric constant, has been considered for improvement in sensor performance for a small variation of refractive index in sensing medium [20–22]. The dielectric constant of metals plays a vital role in the selection of SPR active metals. However, gold (Au) is preferred over Ag due to high chemical stability and resistivity for oxidation but poor molecule binding ability of the Au layer limits the performance of the Au-based SPR sensor [12, 23, 24]. In the current study, we have used a $BaTiO_3$ layer between the silver and graphene layers: three affinity layers, namely nicotine, toluene, and poly (trifluoroethyl methacrylate) with graphene for *Pseudomonas* detection in the proposed structure.

The proposed sensor structure with different affinity layers may be suitable in the detection of other water-contaminating bacteria *Escherichia coli*, *Salmonella*, etc., but in the current study, we have focused on the *Pseudomonas* bacterial detection. Various performance parameters such as sensitivity, quality parameter, and detection accuracy are obtained for the proposed structure to exhibit its performance.

This paper is structured as follows: section 2 gives the design consideration and methodology of the proposed sensor structure. The result and discussion for the proposed structure have been described in section 3. Section 4 gives the conclusion of this work.

Structure Consideration and Methodology

The structure of the proposed biosensor is shown in Fig. 1a. In our design, we have used a BK7 glass prism to couple light and He-Ne laser of $\lambda = 633$ nm wavelength as a light source. The value of the refractive index of BK7 glass prism is 1.5151 which can be calculated by the following relation [25]:

$$n_{BK7} = \left(1 + \frac{1.03961212\lambda^2}{\lambda^2 - 0.00600069867} + \frac{1.01046945\lambda^2}{\lambda^2 - 103.560653} + \frac{0.231792344\lambda^2}{\lambda^2 - 0.0200179144}\right)^{\frac{1}{2}} \quad (1)$$

The design consists of silver as a first layer having a thickness (d_{Ag}) of 50 nm grown on BK7 glass prism. The refractive index of this layer is 0.056206 + 4.2776i [26].

The barium titanate is further deposited as the second layer over the silver layer. The optimum value of the thickness of this layer is $d_{BaTiO3} = 5$ nm. The refractive index of this layer is 2.4042 [27]. Further, the third layer graphene having a thickness ($d_{graphene}$) of 0.34 nm is deposited over barium titanate. The value of the refractive index ($n_{graphene}$) of graphene can be obtained from the following relation [28]:

$$n_{graphene} = 3 + \lambda \frac{C}{3} i \quad (2)$$

Where the value of constant C is 5.446 μm^{-1}.

The detection mechanism involves the adsorption of *Pseudomonas* bacteria on the surface of the graphene layer with the help of the affinity layer. In our proposed SPR structure, the sensing medium is chosen as water having a refractive index of 1.33. The refractive index of the sensing medium varies from 1.33 to 1.40 due to the presence of *Pseudomonas* bacteria and this variation in the refractive index of the sensing medium depends on the culture concentration and motility of *Pseudomonas* bacteria [4]. The fourth layer is the affinity layer. To detect *Pseudomonas* bacteria, we have considered affinity layers with three different values of refractive index, i.e., 1.5265 (nicotine), 1.49368 (toluene), and 1.4370 [poly (trifluoroethyl methacrylate)] [4]. The optimum thickness (d_{aff}) of the affinity layer has been considered 3 nm. The optimum thickness and refractive index of each layer are shown in Table 1 for the proposed structure.

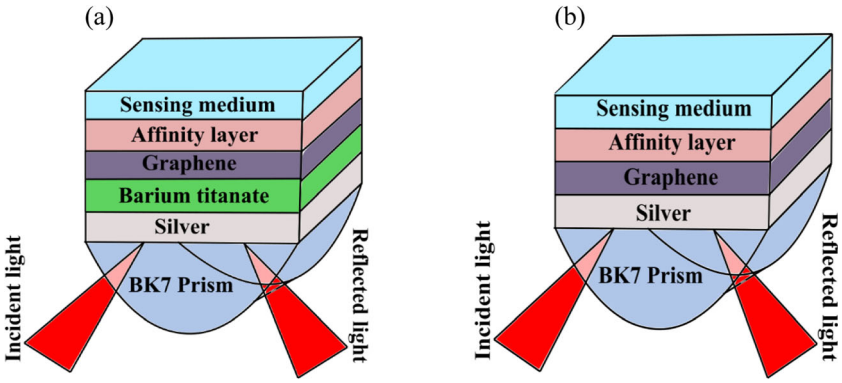

Fig. 1 Structure of (**a**) proposed Ag-$BaTiO_3$-graphene-affinity layer–based SPR biosensor; (**b**) Ag-graphene-affinity layer–based SPR biosensor

Figure 1b shows the SPR biosensor without the barium titanate layer. All the parameters in this structure have the same values as in the proposed SPR biosensor with the barium titanate layer.

In this article, the angular modulation approach has been used for the study of the proposed structure. Here, we have used the Fresnel multilayer reflection theory and transfer matrix method to analyze the reflectivity of p− polarized incident light wave. To excite surface plasmon, propagation constants of p− polarized (TM wave) incident light (k_{in}) and surface plasmon (k_{sp}) should be equal. Mathematically [29]:

$$k_{in} = k_{sp} \tag{3}$$

$$\frac{\omega}{c}\sqrt{\varepsilon_{pr}}\sin\theta_{in} = \frac{\omega}{c}\sqrt{\frac{\varepsilon_m\varepsilon_d}{\varepsilon_m+\varepsilon_d}} \tag{4}$$

Where ε_{pr} is the dielectric permittivity of the prism, ω is the angular frequency, ε_m is the dielectric permittivity of metal, θ_{in} is the angle of the incident light, and $\varepsilon_d$is the dielectric permittivity of the dielectric layer.

Here, all N layers are arranged in a stack along the z-axis. For each layer, dielectric constant and thickness are ε_k and d_k respectively. Tangential field of the first boundary is at $z = 0$ and the tangential field of the final boundary is at $z = z_{N-1}$. Mathematically [30]:

$$\begin{bmatrix} P_1 \\ V_1 \end{bmatrix} = M \begin{bmatrix} P_{N-1} \\ V_{N-1} \end{bmatrix} \tag{5}$$

Where, P_1 and P_{N-1} are the tangential fields of the electric field at first layer boundary and N^{th} layer boundary respectively, V_1 and V_{N-1} are the tangential fields of the magnetic field at first layer boundary and N^{th} layer boundary respectively. For N-layer structure, characteristic matrix (M) can be given as:

$$M = \left(\sum_{k=2}^{N-1} M_k\right)_{ij} = \begin{bmatrix} M_{11} & M_{12} \\ M_{21} & M_{22} \end{bmatrix} \tag{6}$$

$$\text{Where } M_k = \begin{bmatrix} \cos\beta_k & (-i\sin\beta_k)/q_k \\ -iq_k\sin\beta_k & \cos\beta_k \end{bmatrix} \tag{7}$$

With, $q_k = (\varepsilon_k - n_1^2\sin^2\theta_1)^{1/2}/\varepsilon_k$ and $\beta_k = \frac{2\pi d_k}{\lambda}\left(\varepsilon_k - n_1^2\sin^2\theta_1\right)^{1/2}$, in which λ is the incident light wavelength and θ_1 is the angle of the incident light. Matrix elements M_{11}, M_{12}, M_{21}, and M_{22} can be obtained by applying transfer matrix method; the total reflection coefficient (r_p) for TM wave (p− polarized light) can be given as:

$$r_p = \frac{q_1(M_{11} + M_{12}q_N) - (M_{21} + M_{22}q_N)}{q_1(M_{11} + M_{12}q_N) + (M_{21} + M_{22}q_N)} \tag{8}$$

And finally, reflectivity (R) for hybrid N-layer structure can be expressed by:

$$R = r_p r_p^{*} = |r_p|^2 \tag{9}$$

The performance of a sensor can be characterized mainly for sensitivity, quality parameter, and sensor accuracy. The sensitivity of the SPR biosensor can be specified for the angle, phase, wavelength, and polarization or intensity modulation [31, 32]. Angular sensitivity (S_θ) of the SPR-based sensor can be expressed in terms of resonance angle change ($\delta\theta_{res}$) and refractive index change (δn_s). Mathematically [33]:

Table 1 Design parameters of materials used in the proposed SPR biosensor at $\lambda = 633$ nm

S. No.	Name of material	Refractive index of material	Optimum thickness of material
1.	Silver	0.056206 + 4.2776i	50 nm
2.	Barium titanate	2.4042	5 nm
3.	Graphene	3 + 1.149106i	0.34 nm
4.	Affinity layer	1.4370/1.49368/1.5265	3 nm

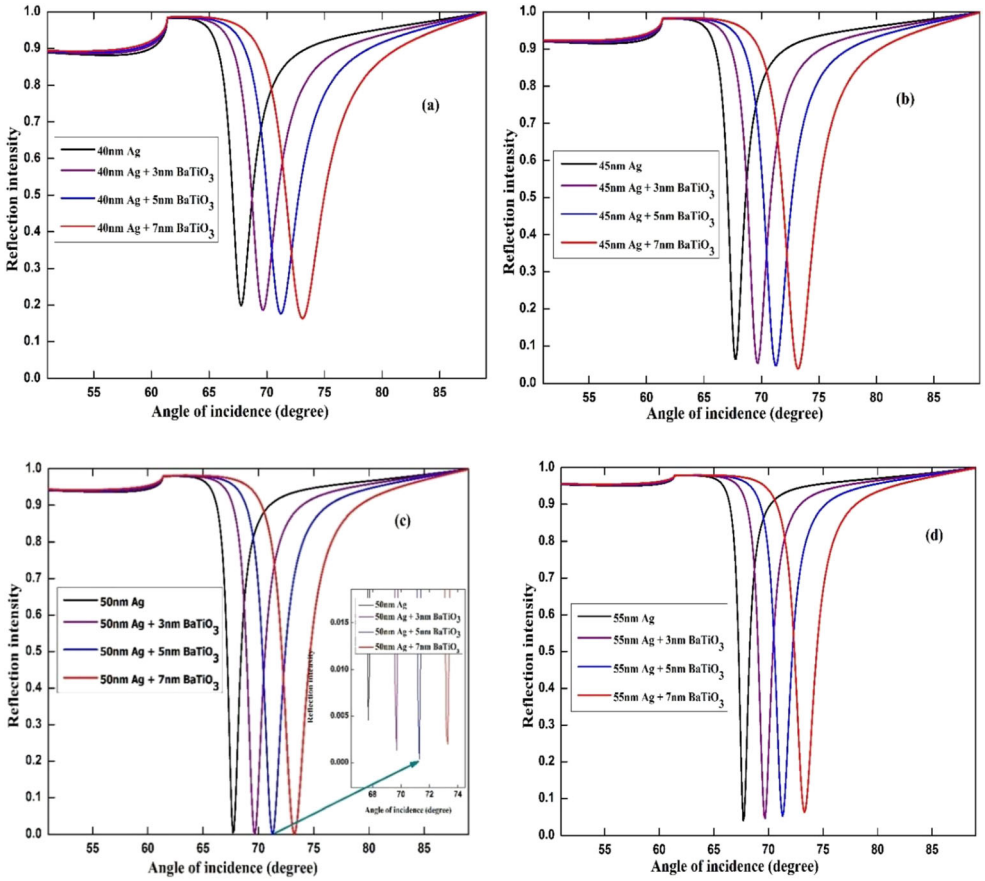

Fig. 2 Reflection spectra for minimum intensity with different thicknesses of Ag layer for (**a**) 40 nm of Ag layer; (**b**) 45 nm of Ag layer; (**c**) 50 nm of Ag layer; (**d**) 55 nm of Ag layer with 0 nm of $BaTiO_3$ layer (without $BaTiO_3$ layer), 3 nm of $BaTiO_3$ layer, 5 nm of $BaTiO_3$ layer, 7 nm of $BaTiO_3$ layer, and constant thickness of graphene layer ($d_{Graphene}$) = 0.34 nm and sensing medium 1.33

$$S_\theta = \frac{\delta\theta_{res}}{\delta n_s} \tag{10}$$

Here, angular sensitivity is expressed in degree per RIU for the angular modulation approach.

Quality parameter (Q) or figure of merit (FOM) for SPR-based sensors can be given in terms of sensitivity and FWHM as follows:

$$Q = \frac{S_\theta}{FWHM} \tag{11}$$

It is usually expressed in (RIU^{-1}).

Another important performance parameter of a sensor is detection accuracy or signal to noise ratio (SNR). It can be expressed in terms of resonance angle change ($\delta\theta_{res}$) and FWHM and can be written as:

$$\text{Detection accuracy} = \frac{\delta\theta_{res}}{FWHM} \tag{12}$$

FWHM can be obtained from the SPR curve where the spectral width is at 50% reflection intensity.

Result and Discussion

The proposed structure of SPR biosensor based on Ag-$BaTiO_3$-graphene for *Pseudomonas* bacterial detection is

Table 2 Optimized values of thickness of the Ag and $BaTiO_3$ layer for minimum reflectivity (R_{min}) used in the proposed SPR biosensor

Thickness of Ag layer (d_{Ag}) (nm)	Thickness of $BaTiO_3$ layer (d_{BaTiO3}) (nm)	Resonance angle (θ_{SPR}) (degree)	Minimum reflectivity (R_{min})
40	0	67.79	0.1977
40	3	69.69	0.1856
40	5	71.19	0.176
40	7	73.09	0.1632
45	0	67.79	0.06421
45	3	69.69	0.05332
45	5	71.29	0.04697
45	7	73.19	0.03781
50	0	67.69	0.00458
50	3	69.69	0.001328
50	5	71.29	0.0003537
50	7	73.29	0.002
55	0	67.69	0.04074
55	3	69.69	0.04659
55	5	71.29	0.0528
55	7	73.29	0.06376

shown in Fig. 1a. The performance analysis of the proposed structure is based on numerical simulation. The structure consists of optimum thicknesses of different layers as given in Table 1. Here, the thickness of each layer in the proposed structure has been optimized for the best performance of the sensor.

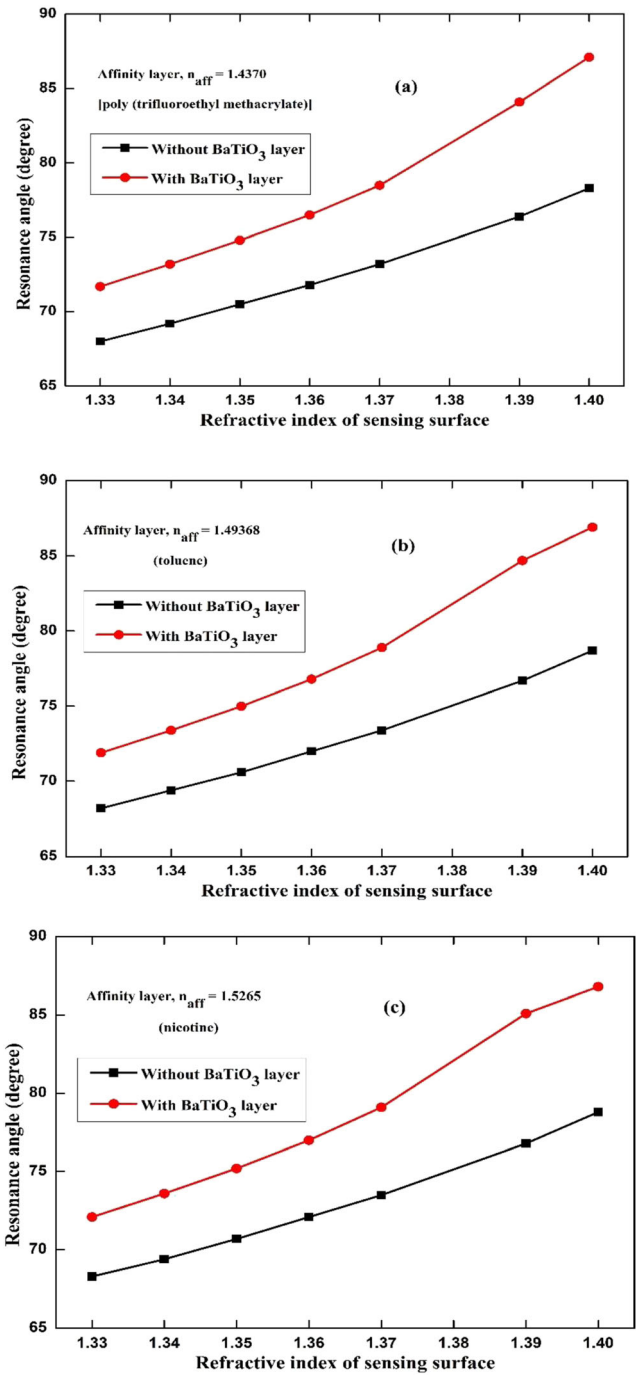

Fig. 3 Spectra of resonance angle variation with refractive index of the proposed structure (symbol at red line) having thicknesses of d_{Ag} = 50 nm, d_{BaTiO3} = 5 nm, and $d_{graphene}$ = 0.34 nm, and structure without barium titanate (symbol at black line) having thicknesses of d_{Ag} = 50 nm, $d_{graphene}$ = 0.34 nm, and sensing medium of refractive index 1.33 for (**a**) affinity layer of refractive index n_{aff} = 1.4370 [poly (trifluoroethyl methacrylate)], (**b**) affinity layer of refractive index n_{aff} = 1.49368 (toluene), (**c**) affinity layer of refractive index n_{aff} = 1.5265 (nicotine)

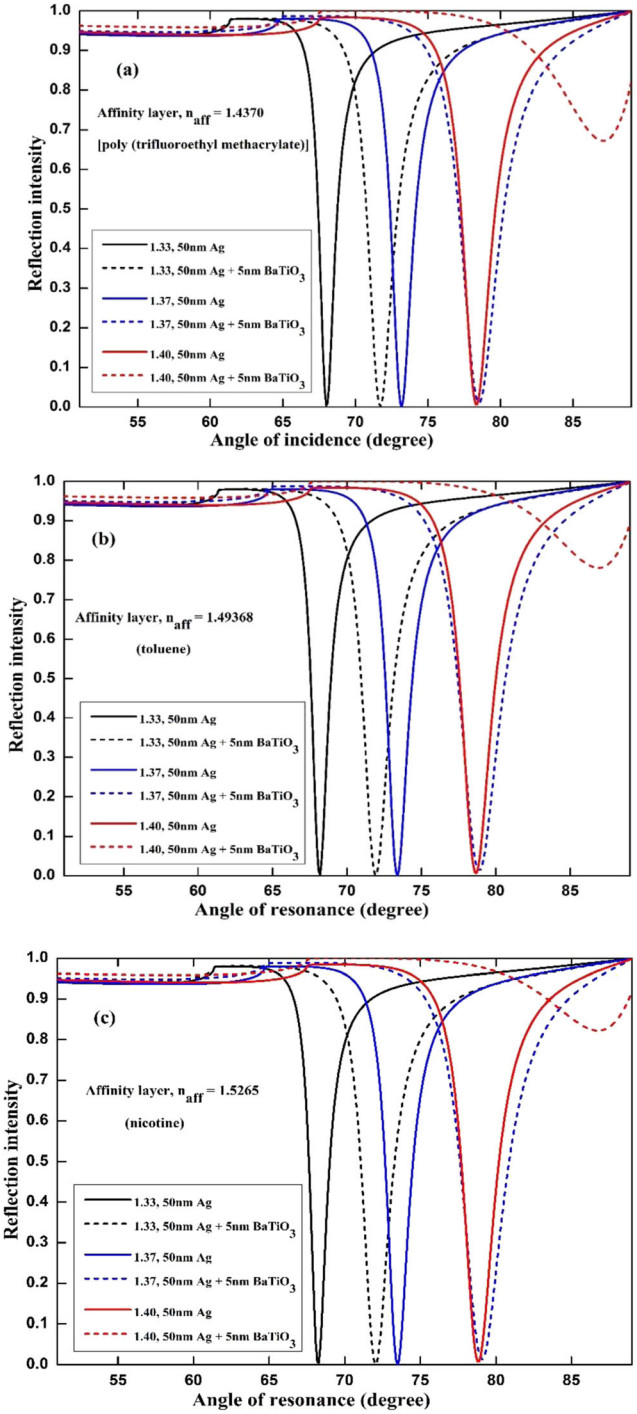

Fig. 4 Reflection spectra of the proposed structure (dash line) having thicknesses of d_{Ag} = 50 nm, d_{BaTiO3} = 5 nm, and $d_{Graphene}$ = 0.34 nm, and structure without $BaTiO_3$ layer (solid line) having thicknesses of d_{Ag} = 50 nm and $d_{Graphene}$ = 0.34 nm and sensing medium of refractive index 1.33 for (**a**) affinity layer of refractive index n_{aff} = 1.4370 [poly (trifluoroethyl methacrylate)], (**b**) affinity layer of refractive index n_{aff} = 1.49368 (toluene), and (**c**) affinity layer of refractive index n_{aff} = 1.5265 (nicotine)

Table 3 Comparison of performance parameters (sensitivity, quality parameter, and detection accuracy) of the proposed SPR biosensor with and without the $BaTiO_3$ layer

Refractive index of affinity layer (n_{aff})	Without the $BaTiO_3$ layer			With $BaTiO_3$ layer		
	Sensitivity (S_θ) (degree/RIU)	Quality parameter (Q) (RIU^{-1})	Detection accuracy (D.A.)	Sensitivity (S_θ) (degree/RIU)	Quality parameter (Q) (RIU^{-1})	Detection accuracy (D.A.)
1.4370	147.14	110.63	7.74	220	101.38	7.09
1.49368	150	110.29	7.72	214.28	96.52	6.75
1.5265	150	109.48	7.66	210	93.75	6.56

Initially, we have investigated the effect of the thickness of both silver and barium titanate layers for minimum reflectivity at a fixed wavelength of 633 nm. Figure 2a–d represent the reflection spectra for different thicknesses for Ag and $BaTiO_3$ layers and the variation of reflectivity with thickness. In Fig. 2a, we have considered the 40 nm thickness of the Ag layer with 0 nm of $BaTiO_3$ layer (without $BaTiO_3$ layer), 3 nm of $BaTiO_3$ layer, 5 nm of $BaTiO_3$ layer, and 7 nm of $BaTiO_3$ layer. Further, Fig. 2b shows the reflection intensity curve for 45 nm thickness of the Ag layer with 0 nm of $BaTiO_3$ layer (without $BaTiO_3$ layer), 3 nm of $BaTiO_3$ layer, 5 nm of $BaTiO_3$ layer, and 7 nm of $BaTiO_3$ layer. Figure 2c gives the reflection intensity curve for 50 nm of the Ag layer with 0 nm of $BaTiO_3$ layer (without $BaTiO_3$ layer), 3 nm of $BaTiO_3$ layer, 5 nm of $BaTiO_3$ layer, and 7 nm of $BaTiO_3$ layer while Fig. 2d shows the reflectivity curve for 55 nm of the Ag layer with 0 nm of $BaTiO_3$ layer (without $BaTiO_3$ layer), 3 nm of $BaTiO_3$ layer, 5 nm of $BaTiO_3$ layer, and 7 nm of $BaTiO_3$ layer. In the proposed design while optimizing the Ag and $BaTiO_3$ layers, the thickness of the graphene layer with sensing medium water was kept constant at 0.34 nm in each case. The value of the minimum reflectivity (R_{min}) and resonance angle in each case are shown in Table 2. In Fig. 2c, the value of minimum reflectivity(R_{min}) is 0.0003537, which is least among all the cases as shown in Table 2. Hence, the optimum values of thickness of the Ag layer and $BaTiO_3$ layer are 50 nm and 5 nm respectively for the graphene layer of thickness 0.34 nm and sensing medium 1.33.

Figure 1b represents the structure of the SPR biosensor without the $BaTiO_3$ layer. In Fig. 3a–c, the variation of resonance angle with the change in concentration of *Pseudomonas* bacteria for three different affinity layers is shown. In Fig. 3a, the plot between the refractive index of the sensing medium and resonance angle variation for [poly (trifluoroethyl methacrylate)] affinity layer is shown. Here, resonance angles shift from 67.99° to 71.69°, 69.19° to 73.19°, 70.49° to 74.79°, 71.79° to 76.49°, 73.19° to 78.49°, 76.39° to 84.09°, and 78.29° to 87.09° for refractive indexes 1.33, 1.34, 1.35, 1.36, 1.37, 1.39, and 1.40 respectively. Figure 3b represents the resonance angle variation with the refractive index change in the sensing medium for the toluene affinity layer. Here, resonance angle shifts have been observed from 68.19° to 71.89°, 69.39° to 73.39°, 70.59° to 74.99°, 71.99° to 76.79°, 73.39° to 78.89°, 76.69° to 84.69°, and 78.69° to 87.09° for refractive indexes 1.33, 1.34, 1.35, 1.36, 1.37, 1.39, and 1.40 respectively. While in Fig. 3c, the resonance angle shifts from 68.29° to 72.09°, 69.39° to 73.59°, 70.69° to 75.19°, 72.09° to 76.99°, 73.49° to 79.09°, 76.79° to 85.09°, and 78.79° to 86.79° have been observed for sensing medium having refractive indexes 1.33, 1.34, 1.35, 1.36, 1.37, 1.39, and 1.40 respectively for nicotine affinity layer. Hence, it is evident that the $BaTiO_3$ layer has a significant effect on shifting resonance angle for different concentrations of *Pseudomonas* bacteria.

Figure 4a–c show the plots of reflection spectra for the proposed SPR biosensor and SPR biosensor without the

Table 4 Comparison of the performance parameters (sensitivity, quality parameter, and detection accuracy) of the proposed SPR biosensor with relevant work

Reference	Refractive index of affinity layer (n_{aff})	Sensitivity (S_θ) (degree/RIU)	Quality parameter (Q) (RIU^{-1})	Detection accuracy
This work	1.4370	220	101.38	7.09
	1.49368	214.28	96.52	6.75
	1.5265	210	93.75	6.56
[4]	1.4370	187.43	29.33	2.05
	1.49368	186	28.66	2.00
	1.5265	184.6	28.17	1.97
[5]	1.4370	38.4945	28.5144	1.9960
	1.49368	38.74843	28.2835	1.9798
	1.5265	38.88757	28.1793	1.97
[6]	1.4370	33.98	2.7802	0.2987

$BaTiO_3$ layer for three different affinity layers. Here, we have considered three refractive indexes 1.33, 1.37, and 1.40 of sensing medium.

In Fig. 4a, the reflection spectra for the affinity layer [poly (trifluoroethyl methacrylate)] are shown. Resonance dips are observed at 71.69°, 78.49°, and 87.09° for the proposed biosensor. The value of FWHM for the proposed SPR sensor has been obtained (2.17). From this observation, sensitivity, quality parameter, and detection accuracy of the proposed biosensor for affinity layer [poly (trifluoroethyl methacrylate)] are obtained as 220 degree/RIU, 101.38 RIU^{-1}, and 7.09 respectively. For SPR biosensor without $BaTiO_3$ layer, resonance dips are observed at 67.99°, 73.19°, and 78.29°. Sensitivity, quality parameter, and detection accuracy for SPR biosensor without $BaTiO_3$ layer have been obtained 147.14 degree/RIU, 110.63 RIU^{-1}, and 7.74 respectively.

In the second case, the reflection spectra for the toluene affinity layer are shown in Fig. 4b. For this affinity layer in the proposed SPR biosensor, FWHM is 2.22 and resonance dips are observed at 71.89°, 78.89°, and 86.89°. Sensitivity, quality parameter, and detection accuracy are obtained as 214.28 degree/RIU, 96.52 RIU^{-1}, and 6.75 respectively. For SPR biosensor without $BaTiO_3$ layer, resonance dips are observed at angles 68.19°, 73.39°, and 78.69°. Sensitivity, quality parameter, and detection accuracy for this structure have been calculated 150 degree/RIU, 110.29 RIU^{-1}, and 7.72 respectively.

Further, in the last case, the affinity layer of nicotine has been considered in the proposed SPR biosensor structure. The plot of reflection spectra for this structure is shown in Fig. 4c. For this layer in the proposed SPR biosensor structure, the value of FWHM is 2.24 and reflection dips have been observed at angles 72.09°, 79.09°, and 86.79°. Sensitivity, quality parameter, and detection accuracy are obtained as 210 degree/RIU, 93.75 RIU^{-1}, and 6.56 respectively. For SPR biosensor without $BaTiO_3$ layer, resonance dips are observed at angles 68.29°, 73.49°, and 78.79°. Sensitivity, quality parameter, and detection accuracy for this structure was found 150 degree/RIU, 109.48 RIU^{-1}, and 7.66 respectively. We have concluded that poly (trifluoroethyl methacrylate) affinity layer shall provide the maximum sensitivity while matching the requisite index variation showing the presence of such bacteria.

The performance parameters of the proposed sensor and the SPR sensor without the $BaTiO_3$ layer have been compared and are given in Table 3. Furthermore, we have compared the performance parameters of the proposed sensor structure with other previously related work, which is shown in Table 4.

We have also investigated the performance of the proposed sensor with the increasing number of the graphene layer. For this, we have plotted the reflectivity curve for the increasing number of graphene layers. Figure 5 shows that when we increase the number of graphene layers for three different affinity layers, the minimum reflection intensity increases. It is also clear from the given plot that the minimum reflectivity

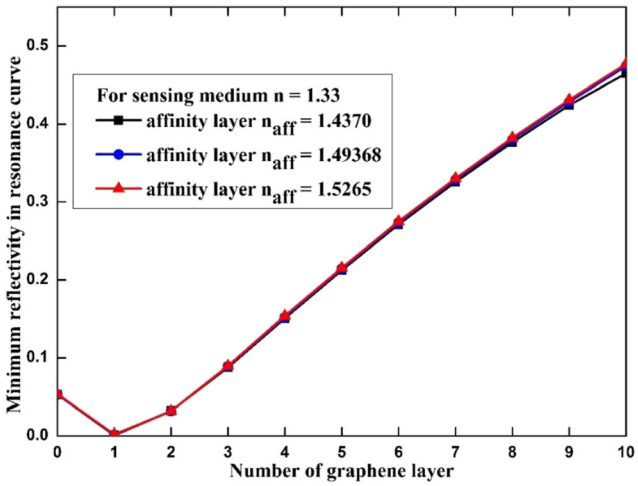

Fig. 5 Plot of minimum reflectivity with number of graphene layer with thickness of $d_{Ag} = 50$ nm, $d_{BaTiO3} = 5$ nm, $d_{graphene} = 0.34$ nm (monolayer), and $d_{aff} = 3$ nm and sensing medium of refractive index 1.33

is high without considering the graphene layer. Hence, monolayer of graphene can be the best choice for the absorption of *Pseudomonas* bacteria with affinity layer.

Meanwhile, to see the effect of thickness of the affinity layer on the performance of the sensor, we have also plotted the shift of resonance angle for different values of thickness of the affinity layer as shown in Fig. 6. It shows the maximum shift in resonance angle for 3 nm thickness of different affinity layers. The maximum resonance angle shift for [poly (trifluoroethyl methacrylate)] affinity layer, toluene affinity layer, and nicotine affinity layer are found to be at 15.40°, 15°, and 14.70° respectively. Hence, affinity layer of 3 nm is considered for the absorption of *Pseudomonas* bacteria with the help of the monolayer of graphene.

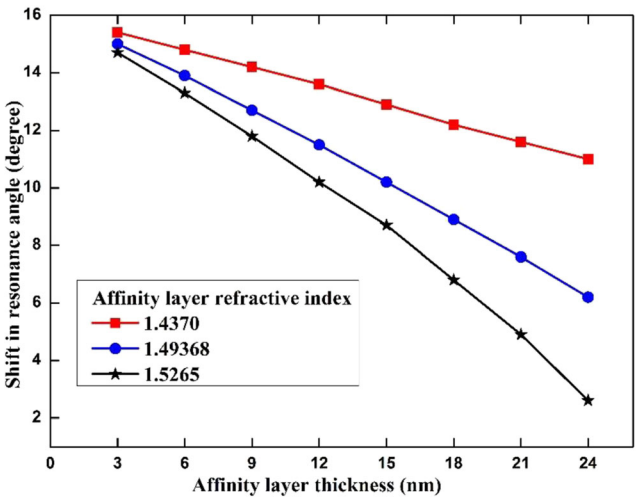

Fig. 6 Plot of the shift in resonance angle as a function of the thickness of affinity layer with thicknesses of $d_{Ag} = 50$ nm, $d_{BaTiO3} = 5$ nm, $d_{graphene} =$ 0.34 nm (monolayer), $d_{aff} = 3$ nm, 13 nm, and 23 nm, and refractive index change from 1.33 to 1.40

Therefore, our proposed SPR biosensor demonstrates enhanced performance in comparison with previously reported work summarized in Table 4.

Conclusion

Our work demonstrates the improved performance in terms of sensitivity, quality parameter, and detection accuracy with the proposed Ag-$BaTiO_3$-graphene-affinity layer–based SPR biosensor. Here, the barium titanate layer, having low dielectric losses and high dielectric constant, has been placed between silver and graphene layers. It is found that graphene with barium titanate enhances the performance when compared with other sensors without the barium titanate layer. Maximum sensitivity, quality parameter, and detection accuracy for this proposed structure are obtained as 220 degree/RIU, 101.38 RIU^{-1}, and 7.09 respectively for change in the refractive index of the sensing medium from $n = 1.33$ to 1.40. This design effectively finds its application in the detection of *Pseudomonas* bacteria and may be useful for sensing in a series of biological analytes.

Acknowledgments Authors are thankful for collaborative work among the members from ECE Department, MNIT Jaipur (India), the Laser Centre, IBNU SINA ISIR, Universiti Teknologi Malaysia, Johor Bahru campus (Malaysia), and the faculty of Applied Sciences, Ton Duc Thang University, Ho Chi Minh City (Vietnam).

References

1. Riveros-Rosas H, Julian-Sanchez A, Moreno-Hagelsieb G, Munoz-Clares RA (2019) Aldehyde dehydrogenase diversity in bacteria of the Pseudomonas genus. Chem Biol Interact 304:83–87. https://doi.org/10.1016/j.cbi.2019.03.006
2. Hossain Z (2014) Bacteria: Pseudomonas. Encycl Food Saf 1:490–500. https://doi.org/10.1016/B978-0-12-378612-8.00109-8
3. Liu T, Hou J, Peng Y (2017) Effect of a newly isolated native bacteria, Pseudomonas sp. NP22 on desulfurization of the low-rank lignite. Int J Miner Process 162:6–11. https://doi.org/10.1016/j.minpro.2017.02.014
4. Kushwaha AS, Kumar A, Kumar R, Srivastava M, Srivastava SK (2018) Zinc oxide, gold and graphene-based surface plasmon resonance (SPR) biosensor for detection of pseudomonas like bacteria: a comparative study. Optik 172:697–707. https://doi.org/10.1016/j.ijleo.2018.07.066
5. Verma A, Prakash A, Tripathi R (2016) Sensitivity improvement of graphene based surface plasmon resonance biosensors with chaclogenide prism. Optik 127:1787–1791. https://doi.org/10.1016/j.ijleo.2015.11.083
6. Verma A, Prakash A, Tripathi R (2015) Performance analysis of graphene based surface plasmon resonance biosensors for detection of Pseudomonas-like bacteria. Opt Quant Electron 47:1197–1205. https://doi.org/10.1007/s11082-014-9976-1
7. Mishra SK, Gupta BD (2012) Surface plasmon resonance-based fiber-optic hydrogen gas sensor utilizing indium–tin oxide (ITO) thin films. Plasmonics 7:627–632. https://doi.org/10.1007/s11468-012-9351-7
8. Shushama KN, Rana MM, Inum R, Hossain MB (2017) Graphene coated fiber optic surface plasmon resonance biosensor for the DNA hybridization detection: simulation analysis. Opt Commun 383:186–190. https://doi.org/10.1016/j.optcom.2016.09.015
9. Kabiraz DC, Morita K, Sakamoto K, Takahashi M, Kawaguchi T (2018) Highly sensitive detection of clenbuterol in urine sample by using surface plasmon resonance immunosensor. Talanta 186:521–526. https://doi.org/10.1016/j.talanta.2018.04.011
10. Zhou J, Qi Q, Wang C, Qian Y, Liu G, Wang Y, Fu L (2019) Surface plasmon resonance (SPR) biosensors for food allergen detection in food matrices. Biosens Bioelectron 142:111449. https://doi.org/10.1016/j.bios.2019.111449
11. Rahman MS, Hasan MR, Rikta KA, Anower MS (2018) A novel graphene coated surface plasmon resonance biosensor with tungsten disulfide (WS_2) for sensing DNA hybridization. Opt Mater 75:567–573. https://doi.org/10.1016/j.optmat.2017.11.013
12. Sharma AK, Pandey AK (2018) Blue phosphorene/MoS_2 heterostructure based SPR sensor with enhanced sensitivity. IEEE Photon Technol Lett 30(7):595–598. https://doi.org/10.1109/LPT.2018.2803747
13. Bijalwan A, Singh BK, Rastogi V (2020) Surface plasmon resonance-based sensors using nano-ribbons of Graphene and WSe2. Plasmonics:1–9. https://doi.org/10.1007/s11468-020-01122-w
14. Fletchert M, Loeb GI (1979) Influence of substratum characteristics on the attachment of a marine pseudomonad to solid surfaces. Appl Environ Microbiol 37(1):67–72
15. Choi SH, Kim YL, Byun KM (2011) Graphene-on-silver substrates for sensitive surface plasmon resonance imaging biosensors. Opt Express 19(12):458–466. https://doi.org/10.1364/OE.19.000458
16. Roy K, Padmanabhan M, Goswami S, Sai TP, Ramalingam G, Raghavan S, Ghosh A (2013) Graphene-MoS2 hybrid structures for multifunctional photoresponsive memory devices. Nat Nanotechnol 8(11):826–830. https://doi.org/10.1038/nnano.2013.206
17. Fu H, Zhang S, Chen H, Weng J (2015) Graphene enhances the sensitivity of fiber optic surface plasmon resonance biosensor. IEEE Sensors J 15(10):5478–5482. https://doi.org/10.1109/JSEN.2015.2442276
18. Kumar R, Kushwaha AS, Srivastava M, Mishra H, Srivastava SK (2018) Enhancement in sensitivity of graphene-based zinc oxide assisted bimetallic surface plasmon resonance (SPR) biosensor. Appl Phys A Mater Sci Process 124:235–210. https://doi.org/10.1007/s00339-018-1606-5
19. Bao M, Li G, Jiang D, Cheng W, Ma X (2012) Surface plasmon optical sensor with enhanced sensitivity using top ZnO thin film. Appl Phys A Mater Sci Process 107:279–283. https://doi.org/10.1007/s00339-012-6858-x
20. Fouad S, Sabri N, Jamal ZAZ, Poopalan P (2017) Surface plasmon resonance sensor sensitivity enhancement using gold-dielectric material. Int J Nanoelectron Mater 10:149–158
21. Liu L, Wang M, Jiao L, Wu T, Xia F, Liu M, Kong W, Dong L, Yun M (2019) Sensitivity enhancement of a graphene– barium titanate-based surface plasmon resonance biosensor with an Ag– au bimetallic structure in the visible region. J Opt Soc Am B 36(4):1108–1116. https://doi.org/10.1364/JOSAB.36.001108
22. Sun P, Wang M, Liu L, Jiao L, Du W, Xia F, Liu M, Kong W, Dong L, Yun M (2019) Sensitivity enhancement of surface plasmon resonance biosensor based on graphene and barium titanate layers. Appl Surf Sci 475:342–347. https://doi.org/10.1016/j.apsusc.2018.12.283
23. Gan S, Zhao Y, Dai X, Xiang Y (2019) Sensitivity enhancement of surface plasmon resonance sensors with 2D franckeite nanosheets. Results Phys 13:102320. https://doi.org/10.1016/j.rinp.2019.102320

24. Chen S, Lin C (2016) High-performance bimetallic film surface plasmon resonance sensor based on film thickness optimization. Optik 127(19):7514–7519. https://doi.org/10.1016/j.ijleo.2016.05.085
25. Lin Z, Jiang L, Wu L, Guo J, Dai X, Xiang Y, Fan D (2016) Tuning and sensitivity enhancement of surface plasmon resonance biosensor with graphene covered Au-MoS2-Au films. IEEE Photon J 8(6):1–8. https://doi.org/10.1109/JPHOT.2016.2631407
26. Johnson PB, Christy RW (1972) Optical constants of the noble metals. Phys Rev B 6:4370–4379. https://doi.org/10.1103/PhysRevB.6.4370
27. Wemple SH, Didomenico JM, Camlibel I (1968) Dielectric and optical properties of melt-grown $BaTiO_3$. J Phys Chem Solids 29:1797–1803. https://doi.org/10.1016/0022-3697(68)90164-9
28. Bruna M, Borini S (2009) Optical constants of graphene layers in the visible range. Appl Phys Lett 94(3):031901. https://doi.org/10.1063/1.3073717
29. Yamamoto M (2002) Surface plasmon resonance (SPR) theory. Tutor Rev Polarogr 48:209. https://doi.org/10.5189/revpolarography.48.209
30. Maharana PK, Jha R (2012) Chalcogenide prism and graphene multilayer based surface plasmon resonance affinity biosensor for high performance. Sens Actuators B Chem 169:161–166. https://doi.org/10.1016/j.snb.2012.04.051
31. Zafar R, Nawaz S, Singh G, d'Alessandro A, Salim M (2018) Plasmonics- based refractive index sensor for detection of hemoglobin concentration. IEEE Sensors J 18(11):4372–4377. https://doi.org/10.1109/JSEN.2018.2826040
32. Sahu S, Yupapin PP, Ali J, Singh G (2018) Porous silicon based Bragg-grating resonator for refractive index biosensing. Photonic Sensors 8(3):248–254. https://doi.org/10.1007/s13320-018-0459-z
33. Maurya JB, Prajapati YK, Singh V, Saini JP (2015) Sensitivity enhancement of surface plasmon resonance sensor based on graphene–MoS2 hybrid structure with TiO2–SiO2 composite layer. Appl Phys A Mater Sci Process 121(2):525–533. https://doi.org/10.1007/s00339-015-9442-3